RAA 2016 Vol. **16** No. **11**, 172 (4pp) doi: 10.1088/1674–4527/16/11/172

http://www.raa-journal.org *http://iopscience.iop.org/raa*

***R**esearch in*
***A**stronomy and*
***A**strophysics*

Example-based super-resolution for single-image analysis from the Chang'e-1 Mission

Fan-Lu Wu and Xiang-Jun Wang

State Key Laboratory of Precision Measuring Technology and Instruments, Tianjin University, Tianjin 300072, China; *xdocuxjw@vip.163.com*

Received 2016 April 16; accepted 2016 July 14

Abstract Due to the low spatial resolution of images taken from the Chang'e-1 (CE-1) orbiter, the details of the lunar surface are blurred and lost. Considering the limited spatial resolution of image data obtained by a CCD camera on CE-1, an example-based super-resolution (SR) algorithm is employed to obtain high-resolution (HR) images. SR reconstruction is important for the application of image data to increase the resolution of images. In this article, a novel example-based algorithm is proposed to implement SR reconstruction by single-image analysis, and the computational cost is reduced compared to other example-based SR methods. The results show that this method can enhance the resolution of images using SR and recover detailed information about the lunar surface. Thus it can be used for surveying HR terrain and geological features. Moreover, the algorithm is significant for the HR processing of remotely sensed images obtained by other imaging systems.

Key words: Moon — methods: data analysis — techniques: image processing

1 INTRODUCTION

Because they are affected by imaging conditions, aliasing, noise, etc, imaging systems are unable to obtain all of the information contained in an original scene. The imaging process is influenced by deformation, aliasing, motion blur, downsampling, noise, etc, leading to deterioration in image quality. Therefore, how to effectively enhance the quality of an image has always been a major issue. Possible hardware-based approaches to this problem include decreasing the pixel size and increasing the sensor size (Nasrollahi & Moeslund 2014). The former approach reduces the amount of light that reaches the associated pixel on a sensor, resulting in an increase in shot noise and more sensitivity to diffraction effects. The latter solution increases the capacitance of the system, which slows down the charge transfer rate (Nasrollahi & Moeslund 2014). Therefore, algorithmic-based approaches are suggested.

Super-resolution (SR) algorithms obtain one high-resolution (HR) image from one or more low-resolution (LR) images. They have been applied to many real-world problems in different fields, such as remote sensing (Zhang et al. 2014; Shen et al. 2009), medical image processing (Wang et al. 2014), facial recognition (Liu et al. 2007; Tappen & Liu 2012), image compression and video enhancement (Schultz & Stevenson 1996; Segall et al. 2004; Liao et al. 2015), etc. In these applications, SR algorithms can be broadly divided into two categories: frequency domain algorithms (Tsai & Huang 1984; Tao et al. 2003) and spatial domain algorithms. Based on the number of LR images involved, spatial domain algorithms can be classified into two classes: reconstruction-based algorithms (Peleg et al. 1987; Irani & Peleg 1991; Stark & Oskoui 1989; Schultz & Stevenson 1994) and learning-based algorithms (Freeman et al. 2000, 2002; Yang et al. 2010).

Chang'e-1 (CE-1) operated in a circular orbit about 200 km away from the lunar surface (Li et al. 2010). On 2010 November 20 at 8:49:00 UTC, the first image of the lunar surface taken by a Chinese probe was obtained from the three-line-array CCD stereo camera mounted on CE-1 (Li et al. 2010). The CCD camera acquired a huge amount of images of the lunar surface. The spatial resolution of these images is 120 m. In order to obtain clearer images and find more applications of CE-1 image data, an SR algorithm is studied in this article.

2 METHODOLOGY

SR refers to the problem of obtaining HR images from LR images. Example-based SR algorithms can be described as nearest-neighbor-based (NN-based) estimation, for instance, Freeman et al. (2000, 2002) defined SR as the task of estimating high-frequency details by interpolating the input LR image. This algorithm is implemented by the NN-based estimation of high-frequency patches and improves the resolution of output patches using a Markov network (Geman & Geman 1984). For a given LR image, Freeman et al. (2000, 2002) try to estimate the underlying HR im-

Table 1 The processing time of 11 236 × 228-size images used for testing. Experiments are performed on an i7-920 (2.67 GHz) computer; the unit in the table is second (s).

Image	Bilinear	Bicubic	Freeman et al.	Yang et al.	Proposed
Image1	0.017116	0.019505	1136.599401	1148.975499	104.790039
Image2	0.017361	0.019678	1165.148185	1161.528312	89.463206
Image3	0.023604	0.027330	1159.660434	1157.918911	77.175699
Image4	0.017889	0.020437	1156.180915	1157.503233	75.445608
Image5	0.017469	0.019405	1149.728817	1166.455011	143.737403
Image6	0.017527	0.019825	1145.306959	1166.806744	155.334632
Image7	0.017780	0.020343	1149.138912	1155.224978	143.801935
Image8	0.016720	0.019730	1151.012229	1150.720157	122.001211
Image9	0.016771	0.020261	1158.790603	1161.699256	145.777820
Image10	0.017794	0.020223	1144.350902	1157.647063	160.617616
Image11	0.018372	0.020642	1147.256916	1172.192948	117.642434
Average	0.018037	0.020671	1151.197661	1159.697465	121.435237

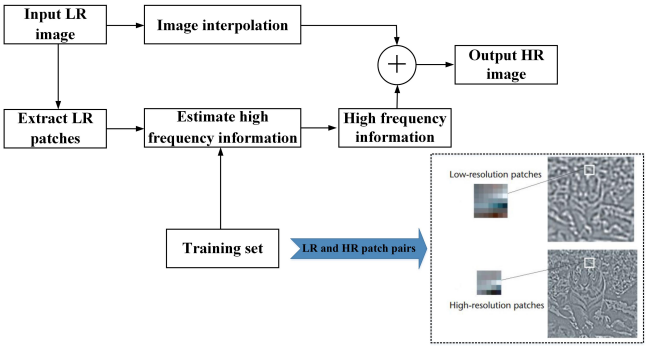

Fig. 1 Main steps in the proposed method.

age. They make the Markov assumption: divide both the LR and HR images into patches, and assign one node of a Markov network to each patch. They draw the network as nodes connected by lines, which indicate statistical dependencies. They connect each HR patch both to its corresponding LR patch and to its spatial neighbors. Since LR and HR are one-to-many mappings, example-based learning strategy with NN-based estimation easily leads to overfitting. Although sparse representation (Yang et al. 2010) is able to compensate the disadvantage of NN-based estimation to some extent, the computational complexity of a large scale dictionary (training data set) is still very high. The sparsity of the solution also depends on the training data.

To solve the problems discussed above, the mapping function between LR and HR images is learned by using the method of regularized regression. Our method is related to kernel ridge regression (An et al. 2007), which has been applied in machine learning and facial recognition, by considering the SR problem as a regression problem. For a given set of training image pairs, we minimize the regularized cost function of the regressor. The time complexity is reduced by finding the minimizer of the regressor only within a sparse subset. A block diagram of the proposed method is illustrated in Figure 1. The key to the

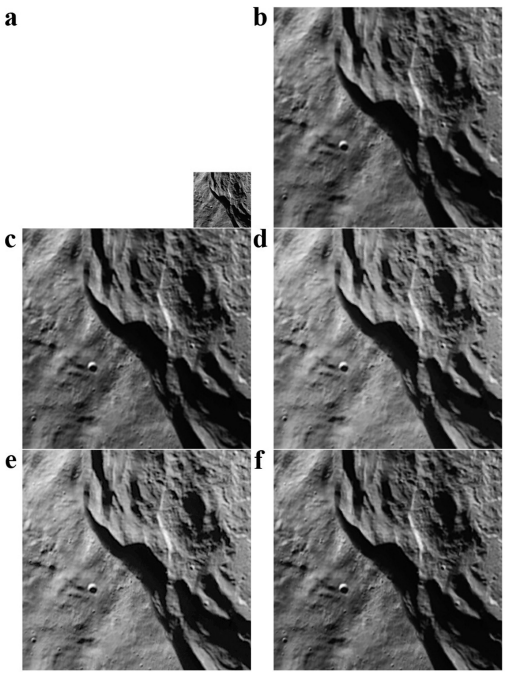

Fig. 2 SR results. (a) Original image (processing time /s). (b) Image obtained by bilinear interpolation (0.016720). (c) Image obtained by bicubic interpolation (0.019730). (d) SR image obtained by Freeman et al.'s algorithm (1151.012229). (e) SR image obtained by Yang et al.'s algorithm (1150.720157). (f) SR image obtained by the proposed algorithm (122.001211).

proposed algorithm is the generated training set. At first, the task seems impossible because high resolution data are missing. In general, the collected images are used as HR images. Then, the set of LR images is obtained by blurring and downsampling the corresponding HR images. The LR pixels are constructed by a weighted combination of HR pixels.

Let us suppose that x_i is an HR patch of size $M\left(\sqrt{M} \times \sqrt{M}\right)$ and y_i is an LR patch of size $N\left(\sqrt{N} \times \sqrt{N}\right)$. For a given set of training data $\left\{(x_1, y_1), \ldots, (x_l, y_l)\right\} \subset R^M \times R^N$, we minimize the following regularized cost function for the regressor $f = \{f^1, \ldots, f^M\}$

$$o(f) = \frac{1}{2}\sum_{i=1}^{M}\left(\sum_{j=1}^{l}\left(f^i(y_j) - x_j^i\right)^2 + \lambda\|f^i\|_H^2\right), \quad (1)$$

where H is a reproducing kernel Hilbert space. Due to the reproducing property, the minimizer of the above function is expanded in kernel functions

$$f^i(\cdot) = \sum_{j=1}^{l} a_j^i k(y_j, \cdot), \quad (2)$$

where k is the reproducing kernel for H. We selected a Gaussian kernel

$$k(x, y) = \exp\left(-\frac{\|x - y\|^2}{\sigma_k}\right). \quad (3)$$

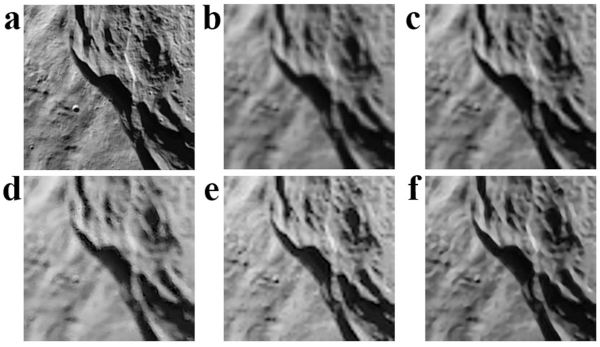

Fig. 3 Results of first downsampling and then generating SR. (a) Original image (PSNR/dB; SSIM; processing time /s). (b) Image obtained by bilinear interpolation (PSNR: 30.8393; SSIM: 0.6136; processing time: 0.007). (c) Image obtained by bicubic interpolation (PSNR: 31.2847; SSIM: 0.6583; processing time: 0.007). (d) SR image obtained by Freeman et al.'s algorithm (PSNR: 24.9447; SSIM: 0.5392; processing time: 71.796). (e) SR image obtained by Yang et al.'s algorithm (PSNR: 24.8333; SSIM: 0.6529; processing time: 69.364). (f) SR image obtained by the proposed algorithm (PSNR: 32.0686; SSIM: 0.7179; processing time: 17.102).

Equation (1) is the sum of individual convex cost functions for each scalar-valued regressor and can be minimized separately. However, by relating the kernel k and regularization parameter λ we can reduce the time complexity of training and testing down to the case of scalar-valued regression because in this case the evaluations of kernel functions can be shared. Plugging Equation (2) into Equation (1) and noting the convexity of Equation (1) yields

$$A = (K + \lambda I)^{-1} X, \tag{4}$$

where $X = [x_1^{\mathrm{T}}, \ldots, x_l^{\mathrm{T}}]^{\mathrm{T}}$ and $[K_{i,j}]_{ll} = k(y_i, y_j)$.

The computational complexity of our approach mainly focuses on finding the optimal sparse subset of the training data set. To reduce the time complexity, a sparse solution is discovered by kernel matching pursuit (KMP) (Vincent & Bengio 2002; Popovici et al. 2005). The basis points of a sparse subset are obtained by an incremental approach: for the first m basis points, the $(m+1)^{\mathrm{th}}$ is obtained through the regularized cost function of the regressor and the matrix which is composed of the coefficients of the regressor.

Our algorithm needs a set of LR and HR image pairs for training. First, we cut out a set of images from the digital orthophoto map (DOM) which is on the scale of 1:2.5 million and is produced by image data obtained from CE-1's CCD camera. Part of these images are used as the HR images of the training set, and other images that belong to the testing set are used as input LR images.

3 RESULTS

The training set has 80 images which have the same size of 236×228, and the testing set has 11 images with the same size. The two sets do not have any intersection. For comparison, several different SR algorithms are applied,

Table 2 The average PSNR, SSIM and processing time for 11 59×57-size images used for testing. Experiments are performed on an i7-920 (2.67 GHz) computer.

Algorithm	PSNR (dB)	SSIM	Time (s)
Bilinear	31.3263	0.6025	0.009003
Bicubic	31.7830	0.6478	0.008495
Freeman et al.	24.6515	0.5447	72.262962
Yang et al.	24.5428	0.6591	70.168818
Proposed	32.3815	0.7013	15.689127

which include the bilinear/bicubic interpolation algorithm, Freeman et al.'s algorithm (Freeman et al. 2002) and Yang et al.'s algorithm (Yang et al. 2010). In this paper, these algorithms are run when the magnification factor is set to 4, and the iterations and k-nearest neighbors are both set to 30. Experimental results are shown in Figure 2. The processing time means the time needed to produce SR which excludes the training time. The processing times of 11 testing images for different algorithms are given in Table 1.

Peak signal-to-noise ratio (PSNR) and structural similarity (SSIM) (Wang et al. 2004) are employed for quantitative comparison. The information loss can be quantitatively assessed by PSNR. SSIM has been widely used for evaluation of the quality of reconstructed images. The value of SSIM is similar to the evaluation of visual interpretation (Zhang et al. 2014; Wang et al. 2004).

$$\mathrm{PSNR} = 10 \times \log_{10}\left(\frac{255^2}{\mathrm{MSE}}\right), \tag{5}$$

$$\mathrm{MSE} = \frac{1}{MN}\sum_{x=0}^{M-1}\sum_{y=0}^{N-1}\left|I_{\mathrm{s}}(x,y) - I_{\mathrm{o}}(x,y)\right|^2, \tag{6}$$

where M and N are the length and width of the images respectively. $I_{\mathrm{s}}(x,y)$ and $I_{\mathrm{o}}(x,y)$ are grey values of the SR image and original image, respectively.

$$\mathrm{SSIM}(x,y) = \frac{(2u_x u_y + C_1)(2\sigma_{xy} + C_2)}{(u_x^2 + u_y^2 + C_1)(\sigma_x^2 + \sigma_y^2 + C_2)}, \tag{7}$$

$$C_1 = (K_1 L)^2, \tag{8}$$

$$C_2 = (K_2 L)^2, \tag{9}$$

where u_x and u_y are the mean values of the SR image and the original image, respectively. σ_x and σ_y represent the variance of the SR image and the original image, respectively. σ_{xy} is the covariance between the SR image and the original image. According to Wang et al. (2004) and Zhang et al. (2014), we set: $K_1 = 0.01$; $K_2 = 0.03$; $L = 255$.

Compared to the above process of taking a 236×228-size image and generating a 944×912 one described above, this experiment first downsampled a 236×228-size image to 59×57 and then produces SR to 236×228. The experimental results are shown in Figure 3. The values of PSNR and SSIM are between the original 236×228-size image and the SR result of a 236×228-size image. The processing time also means the time to yield SR, which excludes

the training time. The average PSNR, SSIM and processing time of 11 testing images for different algorithms are given in Table 2.

4 DISCUSSION AND CONCLUSIONS

In the first set of experiments, the input image is the original 236×228-size image, and only processing time is employed for quantitative comparison. All the example-based SR algorithms outperform the bilinear/bicubic interpolation algorithm (Fig. 2b and Fig. 2c) in terms of visual plausibility. Compared to Freeman et al.'s algorithm (Fig. 2d) and Yang et al.'s algorithm (Fig. 2e), the proposed algorithm improves visual quality of the image (Fig. 2f). Moreover, the proposed algorithm requires much less processing time: about 2 minutes for the proposed algorithm and 19 to 20 minutes for Freeman et al.'s and Yang et al.'s algorithm on the same computer with a 2.67 GHz processor (Table 1).

In the second set of experiments, the input image is the 59×57-size image that was downsampled from the original 236×228-size image. In terms of visual quality, the proposed algorithm produces a less noisy image than the other algorithms (Fig. 3). For quantitative comparison (Table 2), the proposed algorithm outperforms the other algorithms (except in terms of processing time when compared to the interpolation algorithm). Freeman et al.'s algorithm and Yang et al.'s algorithm produce low PSNR values, even lower than the ones produced by the bilinear/bicubic interpolation algorithm. Furthermore, the SSIM of Freeman et al.'s algorithm is also lower than that obtained by the bilinear/bicubic interpolation algorithm. As expected, the proposed algorithm requires much less processing time which is about one-fifth the time cost of Freeman et al.'s and Yang et al.'s algorithm.

This article gives an example-based SR algorithm for a single-image from the CE-1 mission. The mapping function between LR and HR images is learned by using the method of regularized regression, which enriches information on details in images with the computational cost reduced compared to other example-based SR methods. This algorithm is believed to be significant for SR reconstruction of remotely sensed images obtained by other imaging systems. For example, we can select the landing area for the CE-4 mission via SR reconstruction of image data obtained by the Lunar Reconnaissance Orbiter Camera (LROC), which consists of two Narrow Angle Cameras (NACs) and one Wide Angle Camera (WAC). NACs are designed to provide 0.5 meter-scale panchromatic images.

Acknowledgements The authors thank the Ground Research and Application System of the Chinese Lunar Exploration Program for providing data. This study was funded by the National Natural Science Foundation of China (Grant No. 51575388).

References

An, S., Liu, W., & Venkatesh, S. 2007, Pattern Recognition, 40, 2154

Freeman, W. T., Pasztor, E. C., & Carmichael, O. T. 2000, International Journal of Computer Vision, 40, 25

Freeman, W. T., Jones, T. R., & Pasztor, E. C. 2002, IEEE Computer Graphics and Applications, 22, 56

Geman, S., & Geman, D. 1984, IEEE Transactions on Pattern Analysis and Machine Intelligence, 6, 721

Irani, M., & Peleg, S. 1991, CVGIP: Graphical Models and Image Processing, 53, 231

Li, C., Liu, J., Ren, X., et al. 2010, Science China Earth Sciences, 53, 1091

Liao, R., Tao, X., Li, R., Ma, Z., & Jia, J. 2015, in Proceedings of the IEEE International Conference on Computer Vision, 531

Liu, C., Shum, H.-Y., & Freeman, W. T. 2007, International Journal of Computer Vision, 75, 115

Nasrollahi, K., & Moeslund, T. B. 2014, Machine Vision and Applications, 25, 1423

Peleg, S., Keren, D., & Schweitzer, L. 1987, Pattern Recognition Letters, 5, 223

Popovici, V., Bengio, S., & Thiran, J.-P. 2005, Pattern Recognition, 38, 2385

Schultz, R. R., & Stevenson, R. L. 1994, IEEE Transactions on Image Processing, 3, 233

Schultz, R. R., & Stevenson, R. L. 1996, IEEE Transactions on Image Processing, 5, 996

Segall, C. A., Katsaggelos, A. K., Molina, R., & Mateos, J. 2004, IEEE Transactions on Image Processing, 13, 898

Shen, H., Ng, M. K., Li, P., & Zhang, L. 2009, The Computer Journal, 52, 90

Stark, H., & Oskoui, P. 1989, Journal of the Optical Society of America A, 6, 1715

Tao, H., Tang, X., Liu, J., & Tian, J. 2003, in Proc. SPIE, 4898, Image Processing and Pattern Recognition in Remote Sensing, eds. S. G. Ungar, S. Mao, & Y. Yasuoka, 259

Tappen, M. F., & Liu, C. 2012, in European Conference on Computer Vision, Springer, 236

Tsai, R., & Huang, T. S. 1984, Advances in Computer Vision and Image Processing, 1, 317

Vincent, P., & Bengio, Y. 2002, Machine Learning, 48, 165

Wang, Y.-H., Qiao, J., Li, J.-B., et al. 2014, Measurement, 47, 946

Wang, Z., Bovik, A. C., Sheikh, H. R., & Simoncelli, E. P. 2004, IEEE Transactions on Image Processing, 13, 600

Yang, J., Wright, J., Huang, T. S., & Ma, Y. 2010, IEEE Transactions on Image Processing, 19, 2861

Zhang, H., Yang, Z., Zhang, L., & Shen, H. 2014, Remote Sensing, 6, 637